Smart Structures and Systems, *Vol. 29, No. 3 (2022) 457-473*
https://doi.org/10.12989/sss.2022.29.3.457

Experimental study on the effect of EC-TMD on the vibration control of plant structure of PSPPs

Tengfei Zhong [1,2a], Xin Feng*[1,2], Yu Zhang [1,2b] and Jing Zhou [1,2c]

[1] *State Key Laboratory of Coastal and Offshore Engineering, Dalian University of Technology, Liaoning Dalian 116024, China*
[2] *Institute of Earthquake Engineering, Faculty of Infrastructure Engineering, Dalian University of Technology, Dalian, Liaoning, 116024, China*

(*Received April 4, 2021, Revised October 20, 2021, Accepted November 16, 2021*)

Abstract. A high-frequency vibration control method is proposed in this paper for Pumped Storage Power Plants (PSPPs) using Eddy Current Tuned Mass Damper (EC-TMD), based on which a new type of EC-TMD device is designed. The eddy current damper parameters are optimized by numerical simulation. On this basis, physical simulation model tests are conducted to compare and study the effect of structural performance with and without damping, different control strategies, and different arrangement positions of TMD. The test results show that EC-TMD can effectively reduce the control effect under high-frequency vibration of the plant structure, and after the additional damping device forms EC-TMD, the energy dissipation is further realized due to the intervention of eddy current damping, and the control effect is subsequently improved. The Multi-Tuned Mass Damper (MTMD) control strategy broadens the tuning band to improve the robustness of the system, and the vibration advantage is more obvious. Also, some suggestions are made for the placement of the dampers to promote their application.

Keywords: eddy current TMD; high-frequency vibration; plant structure; pumped storage power plants; vibration control

1. Introduction

The development of renewable energy potential is promoted by the high cost of power generation, dependence on fossil fuels and environmental factors in the past decades (Tsioliaridou *et al*. 2006, Kaldellis and Zafirakis 2007, Perez-Sanchez *et al*. 2017). We have recognizing from all walks of life that hydroelectric power generation is not only a renewable and sustainable energy source but also its flexibility and storage capacity to improve the stability of the grid (Rehman *et al*. 2015). It is also a strategic key to ensure the sustainable development of the country (Sun *et al*. 2019). However, with the rapid construction and development of hydropower plants, the capacity of the unit is getting larger and the head is getting higher, and the resulting high-frequency vibration problems of Pumped Storage Power Plants (PSPPs) plants are becoming increasingly prominent (Zhang *et al*. 2018). It is generally recognized that the main vibration source affecting the vibration of the plant structure of PSPPs is the hydraulic vibration source (Amjadian and Agrawal 2017). Due to the complex shape of the worm shell area and incessant transforms in the operating conditions of the power plant, the hydraulic pulsations are characterized by high frequency and complexity that are difficult to control (Ma and Wu 2016). The complex hydraulic pulsation is prone to cause high-frequency resonance of the higher-order modes of the plant structure, which further aggravate the vibration of the plant structure. Therefore, the research on high-frequency vibration control of the PSPPs plant structure is of great significant for the vibration stability of the units and plants.

In recent years, many PSPPs at home and abroad have experienced serious unit and plant vibration problems, such as Hongshi, Huizhou, Zhanghewan in China and Sayanshushensk hydropower plant in Russia (Ma *et al*. 2001, Seleznev *et al*. 2014, Bian *et al*. 2016, Li *et al*. 2019b). Researchers have conducted studies on the vibration problems of plant structures from different aspects and given some vibration reduction suggestions. Qian *et al*. (2007) suggested to minimize the vibration vitality exchanged by the superstructure with decreasing hydraulic power pulsation weight via replenishing air of the worm rigging runner and tailpipe. Luo *et al*. (2006) proposed systematic measures to reduce the optimal unit operating speed and CFD analysis to suppress the vibration of hydropower units because of the severe vibration and runner cracks. Replenishing air and reducing the optimum unit operating speed can reduce the vibration response of the unit to some extent, but the process of gas replenishment has mismatched of the start-up time, the high cost, noisy, power-consuming, and difficult to arrange, and the reduced speed operation causes energy loss of the unit. To reduce the vibration of the plant superstructure, a method was proposed by adding structural crossbeams and additional steel plate reinforced rib beams (Li and Li 2005).

*Corresponding author, Ph.D., Professor,
E-mail: fengxin@dlut.edu.cn
[a] Ph.D. Student, E-mail: zhongtengfei@mail.dlut.edu.cn
[b] Ph.D., E-mail: eerd_zyu@dlut.edu.cn
[c] Ph.D., E-mail: zhouj@dlut.edu.cn

ISSN: 1738-1584 (Print), 1738-1991 (Online)

Although strengthening the strength of the local members of the structure through reinforcement methods can change the local natural vibration characteristics of the structure, the vibration regulation ability of the plant structure caused by complex high-frequency pressure pulsation in the unit is poor, so the vibration reduction effect is very limited. For the newly-building plant structure, Ma *et al*. (2001) enhances the structural integrity of the plant by strengthening the rigid connection of the columns to improve the plant stiffness to reduce the vibration response. Optimizing the design of the plant structure at the design stage can strengthen the overall vibration resistance of the structure and avoid the low-order mode of the structure in the resonance region, but it still cannot guarantee that the high-order mode of the structure completely avoids the resonance region, and the method does not apply to the existing plant structure. Although the above research provides some ideas on the vibration of the plant structure and proposes control methods to solve the vibration of the plant structure from different perspectives, there are still many problems in the practical application, and the vibration problem still exists objectively, which cannot effectively solve the vibration problems of the existing PSPPs plant structure. Therefore, for the characteristics of high-frequency vibration of the plant structure, it is essential to combine the passive control theory to carry out vibration control research on the plant structure.

Tuned mass dampers are one of the more important types of dampers for passive control, which are attached to the main structure by auxiliary masses, springs, and dampers to suppress structural vibrations. The earliest application of TMDs date to 1909 with the invention of dynamic dampers by Frahm (1909). Since then, researchers have extensively investigated the study of dynamic characteristics and parameter design under different excitations (Hartog 1957, Wiesner 1979, Warburton 1982, Chang 1999, Warnitchai and Hoang 2006, Bakre and Jangid 2007, Marian and Giaralis 2017, Ramezani *et al*. 2017). Hartog (1957) developed closed expressions for the optimal damper parameters, i.e., frequency ratio and damping ratio based on harmonic excitation. Researchers have since demonstrated the effectiveness of TMDs in controlling the response of buildings under wind and seismic excitation (Tributsch and Adam 2012, Elias and Matsagar 2014, Elias and Matsagar 2018). Conventional TMDs have been found many shortcomings in recent years, such as damping fluid leakage and damping adjustment difficulties. The eddy current dampers (ECDs) are a good solution to the above problems (Matsuzaki *et al*. 2000, Sodano and Bae 2004, Sodano *et al*. 2005, Ebrahimi *et al*. 2009, Mohanta *et al*. 2017). Compared with conventional damping, ECD as a noncontact damping mechanism may have a long service life, low maintenance requirements, and insensitive to high temperatures. In addition, their damping ratio can be easily adjusted by changing the magnetic field strength or the air gap between the permanent magnet and the conductor (Li *et al*. 2019a). Pan *et al*. (2016) proposed new ECDs to reduce the medium and high-frequency structural vibrations caused by mechanical systems used in aerospace. The combination of ECDs and TMDs forms a new damping mechanism due to the good damping performance of ECDs overcomes the limitations of conventional damping (Larose *et al*. 1995, Wen *et al*. 2016, Niu *et al*. 2018, Wang *et al*. 2020). EC-TMD improves the damping ratio and robustness of the system, ensuring the tuning performance of the TMD while significantly reducing vibration. However, few explicit studies on structural high-frequency vibration control have been reported, both experimentally and numerically, which provides very limited information for a wide range of high-frequency vibration control applications. However, there are still many structures affected by high-frequency vibration in practical engineering, such as PSPPs plant structures, machining plants and aerospace fields. Therefore, it is essential to study the eddy current TMD for high-frequency vibration control of structures.

In this paper, a high-frequency vibration control method is proposed based on EC-TMD and a new high-frequency EC-TMD device is designed. The parameters of EC-TMD are optimized and designed through numerical simulation. The damping performance of the TMD device under high-frequency vibration of the structure is verified through physical model tests. The control capability of the plant structure under high-frequency vibration is analyzed through shaking table tests. The dynamic characteristics of the plant structure with or without damping are studied, and the influence laws of eddy current damping effect, different TMD control strategies, and different TMD arrangement positions. The vibration damping effects of the proposed methods are studied more systematically, providing a feasible solution for the study of high-frequency vibration control of PSPPs plant structures.

2. Theory and methods

2.1 Theoretical backgrounds

In electromagnetic theory, relative velocity between a copper plate as a conductor and the permanent magnet, the copper plate cuts the magnetic force lines to produce eddy current damping, so that the interaction between the eddy current and magnetic fields impedes the relative motion (Sodano *et al*. 2005). The principal schematic of eddy current damping is shown in Fig. 1.

Because of the eddy current damping, the movement of the TMD mass is retarded and the energy is dissipated. To get the eddy current damping coefficient, assume that the

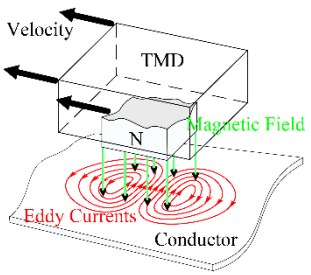

Fig. 1 Principal schematic diagram of Eddy current damping

charge motion on the conductor surface is ignored, the electric current density **J** can be obtained as

$$\boldsymbol{J} = \sigma(v \times \boldsymbol{B}) \tag{1}$$

where σ is the conductive coefficient of the conductive metal, v is the relative velocity of the magnet to the conductive metal, and **B** is the magnetic induction. Assuming that the volume of the conductor plate is V, then the electromagnetic force **F** can be obtained as

$$\boldsymbol{F} = \int_V \boldsymbol{J} \times \boldsymbol{B} \mathrm{d}V \tag{2}$$

In practical use, the movement of the copper plate is assumed perpendicular to the magnetic field. Therefore, by vector calculation, the magnitude f of the eddy current force **F** can be expressed as

$$f = -\sigma\delta SB^2 v \tag{3}$$

$$c_t = \frac{f}{v} = \sigma\delta SB^2 \tag{4}$$

For the high-frequency vibration of the device structure, the high-frequency excitation causes the r-th mode vibration of the structure, and the TMD is designed to control the r-th mode of the structure. The mass, stiffness, and damping matrices of the structure are **M**, **K** and **C,** respectively, and the mass, stiffness and damping of the TMD are m_t, k_t, c_t. the structure and the TMD form a coupled vibration system with N+1 degrees of freedom, and its equations of motion are

$$\begin{aligned}&\boldsymbol{M\ddot{X}} + \boldsymbol{C\dot{X}} + \boldsymbol{KX} - \boldsymbol{\delta_n}\{c_t(\dot{x}_t - \dot{x}_n) + k_t(x_t - x_n)\} \\ &= -\boldsymbol{MI}\ddot{x}_g\end{aligned} \tag{5}$$

$$m_t\ddot{x}_t + c_t(\dot{x}_t - \dot{x}_n) + k_t(x_t - x_n) = -m_t\ddot{x}_g \tag{6}$$

where **X** is the displacement vector of the structure, x_n and x_t are the nth degree-of-freedom of the structure and the absolute displacement of the TMD, respectively, $\ddot{x}_g$ is the ground acceleration, and $\boldsymbol{\delta_n}$ is the TMD installation position vector, except for the nth one, which is 1, and the rest are 0 column vectors. **I** is the load indicator vector of element 1 along the seismic direction and the rest is 0. When the damping is Rayleigh damping, the equation of motion can be decoupled into a single degree of freedom by using modal analysis.

$$\boldsymbol{X} = \boldsymbol{\Phi q} \tag{7}$$

where Φ is the structural vibrational vector matrix and **q** is the generalized coordinate vector. Combining the equations, we get

$$\begin{aligned}&m_r(\ddot{q}_r + 2\zeta_r\dot{q}_r + \omega_r^2 q_r) \\ &-\phi_{rn}\{2\zeta_t\omega_t(\dot{x}_t - \dot{x}_n) + \omega_t^2(x_t - x_n)\} = -\gamma_r m_r\ddot{x}_g\end{aligned} \tag{8}$$

$$m_t[\ddot{x}_t + 2\zeta_t\omega_t(\dot{x}_t - \dot{x}_n) + \omega_t^2(x_t - x_n)] = -m_t\ddot{x}_g \tag{9}$$

where m_r, and ζ_r is the modal mass and damping ratio of the rth of the structure, ω_t and ζ_t are the frequency and damping ratio of the TMD, respectively. ω_r and γ_r are the rth-order intrinsic frequencies and the participation coefficient of the rth-order mode of the structure. ϕ_{rn} is the modal mode displacement of the nth degree of freedom of the rth-order mode. $q_r$is the generalized displacement of the rth order mode.

Then the design problem is essentially similar to the TMD vibration control for a single degree-of-freedom structure. In this way, the higher-order modal vibration control of the plant structure is reduced to the TMD design problem for the corresponding modal coordinates.

Closed-form expression of the optimum damper parameter γ_{opt} is developed by Hartog (1957), which minimizing steady-state response of the main mass subjected to a harmonic main mass excitation. This expression for calculating optimum damper parameters is given as

$$\gamma_{\text{opt}} = \frac{1}{\sqrt{1+\mu}} \tag{10}$$

$$\zeta_{\text{opt}} = \sqrt{\frac{3\mu}{4(2+\mu)(1+\mu)}} \tag{11}$$

where $\gamma_{opt} = \omega_t/\omega_r$ denotes the optimal ratio of TMD frequency to the structure r-order frequency; ζ_{opt} denotes the optimal TMD damping; $\mu = m_t/m_r$ denotes the mass ratio of the TMD to the structure r-order modal mass. Therefore, we can obtain the design parameters of TMD through the optimal frequency ratio. The TMD can be tuned to the best effect using the optimal frequency ratio. In the next section, we will further elaborate on the design, control methods and parameter optimization of TMD.

2.2 Design of EC-TMD

The EC-TMD is composed of a spring, an additional mass, a conductor, and a permanent magnet. When the conductive and the permanent magnet move relative to each other, an eddy current is generated in the conductor. Due to the interaction between the eddy current and the magnetic field of the permanent magnet a repulsive force is generated. In the process of vibration with the structure, the kinetic energy is eventually converted into thermal energy dissipation to achieve structural vibration damping.

For the high-frequency vibration characteristics of the PSPPs plant structure, the natural vibration frequency is high, so it is necessary to design higher frequency TMD devices to reduce the vibration of the structure. Based on the water pressure pulsation characteristics and the transmission path of water pressure pulsation, the vibration of the floor slab is considered reduced by controlling the structural columns so that the vibration energy is dissipated in the transmission path. Therefore, this paper proposes a new EC-TMD vibration reduction device applicable to high-frequency control. It is based on the bending stiffness of the beam and the good deformation capacity of spring steel and achieves the effect of vibration absorption and

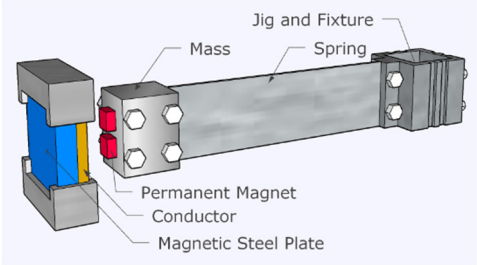

Fig. 2 Eddy current TMD design diagram

energy dissipation by absorbing and dissipating the vibration energy of the structural column, to achieve the purpose of vibration reduction. The concept diagram is shown in Fig. 2.

To simplify the analysis, the steel plant is assumed to be made of the same material, which as cantilever length L, width b, height h, cross-sectional area A, Young's modulus E, density ρ, and quality m_t. The natural frequency of the TMD is calculated via the Rayleigh method (Thomson 1972).

The natural frequency ω_t of the TMD can be calculated as follows

$$\omega_t = \sqrt{\frac{3EI}{m_t L^3 + \frac{33}{140}\rho A L^4}} \tag{12}$$

For PSPPs plant structures, high-frequency pulsating water pressure causes a high-frequency natural vibration of the structure, and the vibration response of the structure is easily observed. Therefore, the high-frequency vibration of the structure is controlled by using dampers, and the structural modes affected by high-frequency vibration are analyzed separately as subsystems, and the specific technical route is shown in Fig. 3. Firstly, the modal identification of the plant structure is carried out to accurately obtain the modal parameters and excitation load parameters of the structure, and to determine the parameter information of the controlled high-frequency modes. Furthermore, the tuning parameters and eddy current damping parameters of the TMD are determined. Study the influence law of important parameters of eddy current damping on the damping coefficient, and optimize the parameters of eddy current damping. Install the EC-TMD device on the plant structure and test the high-frequency vibration response of the structure with and without dampers to evaluate the control performance of the TMD

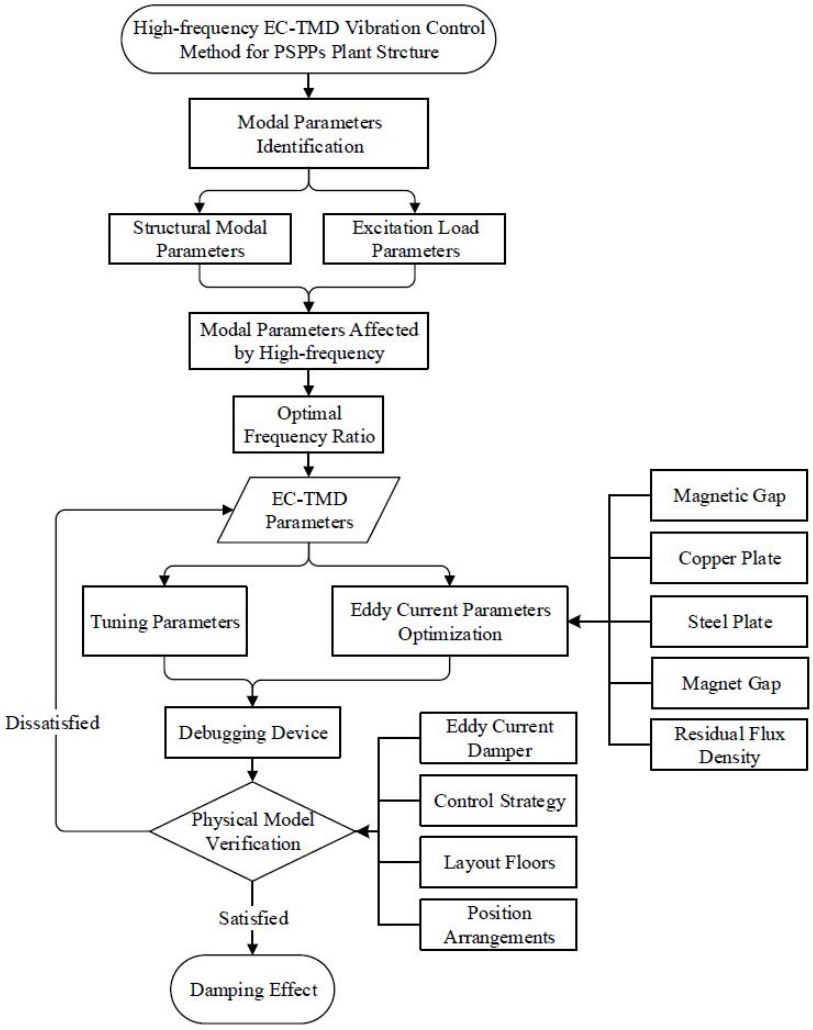

Fig. 3 High-frequency EC-TMD vibration control method for the PSPPs plant structure

device. Moreover, the effects of different control strategies and layout locations on the damping performance are essential. Therefore, in the next tests, the effects of the presence or absence of the damping unit, different control strategies, different layout floors and different layout locations on the high-frequency vibration of the structure are further analyzed.

3. Parameters optimization of eddy current TMD

In this section, a 3D electromagnetic field finite element analysis of the designed EC-TMD damping is performed using COMSOL software to calculate the damping force generated by the eddy current damping, and the corresponding equivalent damping coefficient is used as the performance index of the dampers.

Many factors are affecting the EC-TMD damping performance, such as magnetic field gap, conductive copper plate thickness, permanent magnet residual flux density, permanent magnet gap and permeable steel plate thickness. Taking the new EC-TMD studied in this paper as the object and the damping coefficient as the evaluation index, the influence law of the above parameters on the damping performance of the EC-TMD is analyzed in detail.

3.1 Effect of magnetic field gap

Fig. 4 shows the variation law of the equivalent damping coefficient of eddy current damping with the magnetic field gap for different conductor copper plate sizes. It can be observed from the figure that the equivalent damping coefficient decreases sharply with the increase of the magnetic field gap. Taking the copper plate size of 20 mm as an example, when the magnetic field gap increases from 2 mm to 4 mm, the equivalent damping coefficient decreases from 0.266 N•s/m to 0.070 N•s/m, a decrease of 73.6%; when the magnetic field gap increases from 10 mm to 12 mm, the equivalent damping coefficient decreases from 0.00215 N•s/m to 0.00076 N•s/m, a decrease of 64.6%.

Besides, it can be observed from the figure that the equivalent damping coefficient is positively related to the size of the conductor copper plate when the magnetic field gap is certain. However, when the magnetic field gap reaches a certain width, the equivalent damping coefficient is less affected by different conductor copper plate sizes. When the magnetic field gap is 2 mm, the equivalent damping coefficient increases by 71.6% when the copper plate size increases from 20 mm to 50 mm, and by 19.5% when it increases from 50 mm to 100 mm. Therefore, under the premise of ensuring the normal operation of the dampers, minimizing the magnetic field gap and choosing a reasonable conductor size can not only improve the damping performance of the TMD but also make the structure more compact and improve the economy. The conductor copper plate size of 50 mm is used in the latter.

3.2 Effect of copper thickness

Fig. 5 shows the variation curve of the equivalent damping coefficient with the thickness of the copper plate of the conductor for different magnetic field gaps. From the figure, the equivalent damping coefficient increases sharply with the increase of copper plate thickness and then stabilizes gradually. Taking the magnetic field gap of 2 mm as an example, the equivalent damping coefficient increases from 0.407 N•s/m to 0.936 N•s/m when the thickness of the copper plate increases from 1 mm to 5 mm, an increase of 56.5%; when the magnetic field gap increases from 10 mm to 20 mm, the equivalent damping coefficient increases from 1.025 N•s/m to 1.047 N•s/m, an increase of 0.2%.

Besides, it can be observed from the figure that the equivalent damping coefficient is negatively correlated with the magnetic field gap when the copper plate thickness is certain. It decreases sharply with the increase of the magnetic field gap. However, when the magnetic field gap reaches the width, the equivalent damping coefficient is less affected by different conductor copper plate sizes. When the copper plate thickness is 5 mm, the equivalent damping coefficient decreases by 63.3% when the magnetic field gap is increased from 2 mm to 4 mm, and by 53.4% when it is increased from 8 mm to 10 mm. Therefore, considering the damping effect of the structure and the economy of the device, the thickness of the conductive copper plate is

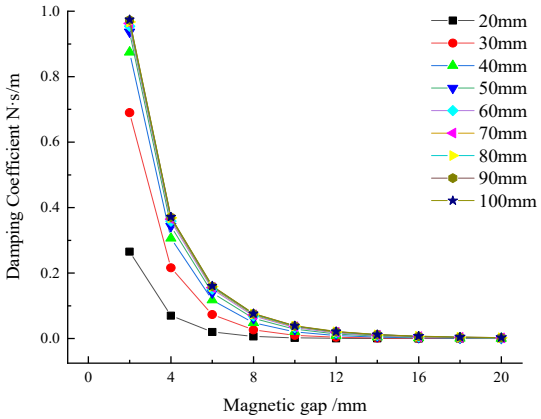

Fig. 4 Damping equivalent damping coefficient with conductor copper plate size, magnetic field gap variation law

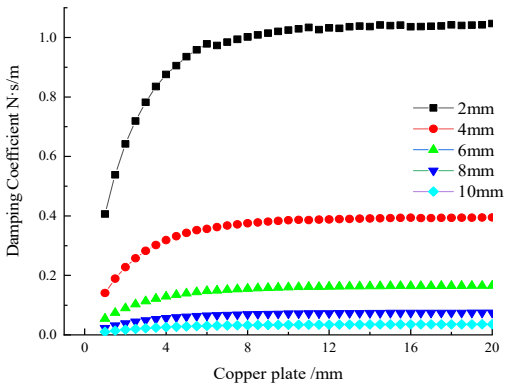

Fig. 5 Variation of equivalent damping coefficient with the thickness of the copper plate conductor for different magnetic field gaps

uniformly taken as 5 mm in the later analysis.

3.3 Effect of magnetic steel plate

The magnetic congregate effect of the magnetic steel plate on the magnetic lines of force of the permanent magnet can significantly enhance the magnetic induction strength around the permanent magnet. Fig. 6 shows the variation of the equivalent damping coefficient with the thickness of the magnetic steel plate for different magnetic field gaps. The equivalent damping coefficient increases significantly after the additional magnetic steel plate. For example, the equivalent damping coefficient increases from 0.936 N•s/m to 1.594 N•s/m when the thickness of the additional magnetic steel plate is 1mm, which is 41.3%. The equivalent damping coefficient gradually increases and then stabilizes with the increasing thickness of the additional magnetic steel plate, and the change of the damping performance is small. The equivalent damping coefficient increases from 1.911 N•s/m to 1.945 N•s/m when the thickness of the additional magnetic steel plate increases from 10 mm to 20 mm, which is only an increase of 1.7%. This is mainly because as the thickness of the magnetic steel plate increases, the distance from the steel plate to the surface of the permanent magnet increases, and the magnetic lines of force gradually decrease, and the amount of magnetization also gradually stabilizes, so further increasing the thickness of the magnetic steel plate has less effect on the equivalent damping coefficient.

Besides, it can be observed from the figure that the equivalent damping coefficient is negatively related to the magnetic field gap when the thickness of the magnetic steel plate is certain. It decreases with the increase of the magnetic field gap. When the thickness of the steel plate is 10 mm, the equivalent damping coefficient decreases by 58.0% when the magnetic field gap increases from 2 mm to 4 mm, and by 46.0% when it increases from 8 mm to 10 mm. In summary, the thickness of the magnetically conductive steel plate should be 10 mm in the later analysis.

The magnetic field distribution of the conductor plate is limited, and the strongest magnetic field in the part close to the permanent magnet, and the magnetic field gradually decreases in the part far from the permanent magnet, so the interference to the adjacent steel plate is negligible.

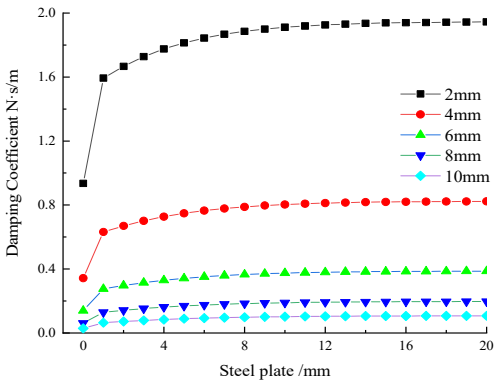

Fig. 6 Variation of equivalent damping coefficient with the thickness of magnetic steel plate for different magnetic field gaps

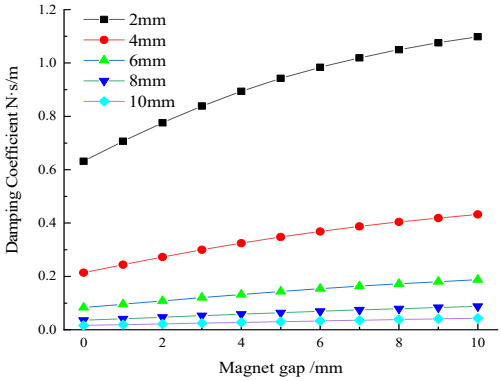

Fig. 7 Variation of the equivalent damping coefficient with the spacing of permanent magnets for different magnetic field gaps

3.4 Effect of the spacing of the permanent magnets

Fig. 7 shows the variation of the equivalent damping coefficient with the spacing of the permanent magnets for different magnetic field gaps. The equivalent damping coefficient increases gradually with the increase of the permanent magnet pitch and then tends to be flat. For example, when the magnetic field gap is 2 mm, the equivalent damping coefficient increases from 0.776 N•s/m to 0.984 N•s/m when the permanent magnet pitch increases from 2 mm to 6 mm, which is an increase of 21.1%, and increases from 0.984 N•s/m to 1.099 N•s/m when the permanent magnet pitch increases from 6 mm to 10 mm, which is an increase of 10.5%.

Besides, it can be observed from the figure that the equivalent damping coefficient is negatively correlated with the magnetic field gap when the permanent magnet spacing is certain. It decreases with the increase of the magnetic field gap. When the permanent magnet pitch is 6 mm, the equivalent damping coefficient decreases by 62.5% when the magnetic field gap increases from 2 mm to 4 mm, and by 52.2% when it increases from 8 mm to 10 mm.

3.5 Effect of the magnetic flux density

Magnetic flux density indicates the number of magnetic lines of force perpendicular to the unit area. It quantitatively reflects the sparsity of the magnetic lines of force. The performance of the magnetic material varies for different types of permanent magnets. Fig. 8 shows the variation of the equivalent damping coefficient with the residual flux density of the permanent magnet for different magnetic field gaps. When the magnetic field gap is small, the equivalent damping coefficient gradually increases with the increase of the residual flux density of the permanent magnet. Taking the magnetic field gap of 2 mm as an example, when the residual flux density increases from 1 T to 1.44 T, the equivalent damping coefficient increases from 0.454 N•s/m to 0.942 N•s/m, an increase of 51.8%.

Also, it can be observed from the figure that the equivalent damping coefficient is negatively related to the

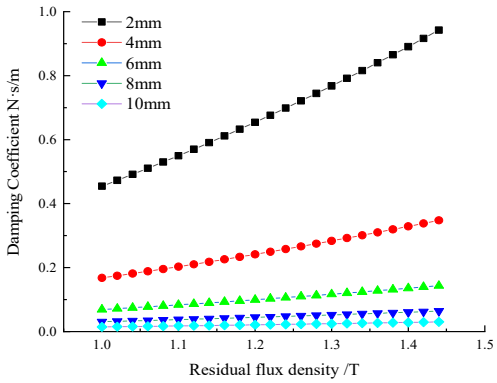

Fig. 8 Variation of equivalent damping coefficient with a residual flux density of permanent magnets for different magnetic field gaps

magnetic field gap when the residual flux density is certain. It decreases with the increase of the magnetic field gap. When the residual flux density is 1.44 T, the equivalent damping coefficient decreases by 63.1% when the magnetic field gap increases from 2 mm to 4 mm, and by 52.5% when it increases from 8 mm to 10 mm. Therefore, the change of magnetic flux density directly affects the number of magnetic lines of force and is an important parameter to improve the damping performance. In this paper, N52 type NdFeB permanent magnets with a residual magnetic flux density of 1.44 T are used.

Three-dimensional electromagnetic field finite element simulation can meet the quantitative calculation and parameter optimization design needs of the equivalent damping coefficient of eddy current damping components. The equivalent damping coefficient of the eddy current damping element improves significantly with the decrease of the magnetic field gap. The distance between the permanent magnet and the conductor plate should be reduced as much as possible. However, to avoid the collision between the TMD device and the eddy current damping member during the motion, and to reduce the adverse effect of the magnetic field attraction between the mass block and the eddy current damping member on the vibration frequency of the TMD, the magnetic field gap should not be taken too small. Therefore, the magnetic field gap is taken as 4 mm, and the damping performance can be improved significantly by attaching a magnetically conductive steel plate to the conductor copper plate due to the magnetic congregation of the plate. The increase of permanent magnet spacing makes the equivalent damping coefficient increase and then stabilize, considering the convenience of permanent magnet installation and the magnetic field gap, the permanent magnet spacing is 6mm. In actual plant structures, the increase in size of the EC-TMD is leading to a significant increase in the equivalent damping coefficient, the magnetic field gap is further adjusted to improve the damping coefficient in combination with the actual demand to achieve the damping target. The specific test program will be discussed in the next section.

4. Experimental setup

To verify the effectiveness of the eddy current TMD control plant structure damping scheme under high-frequency vibration, a series of experiments were designed. The experiments investigate the damping effect of the structure-eddy current damper system under high-frequency vibration and are not limited to the strict similarity of the structural form and transmission path. The experiments in this paper use a three-story steel frame structure to simulate the plant structure and test the vibration response of the structure under high-frequency vibration through the experiments to analyze the effect of control of high-frequency vibration of the structure with or without the damping TMD, different arrangement positions and different control strategies. The experimental model in the paper can be regarded as a microreduced prototype similar to the structure of the PSPPs. The stiffness at the bottom and center of the steel frame is much greater than the structural columns, which is similar to the stiffness distribution of the plant structure. The structure design is shown in Fig. 9. The square steel cylinder in the middle of the bottom level simulates the bulk concrete of the worm shell layer of the plant structure, and the steel cylinders in

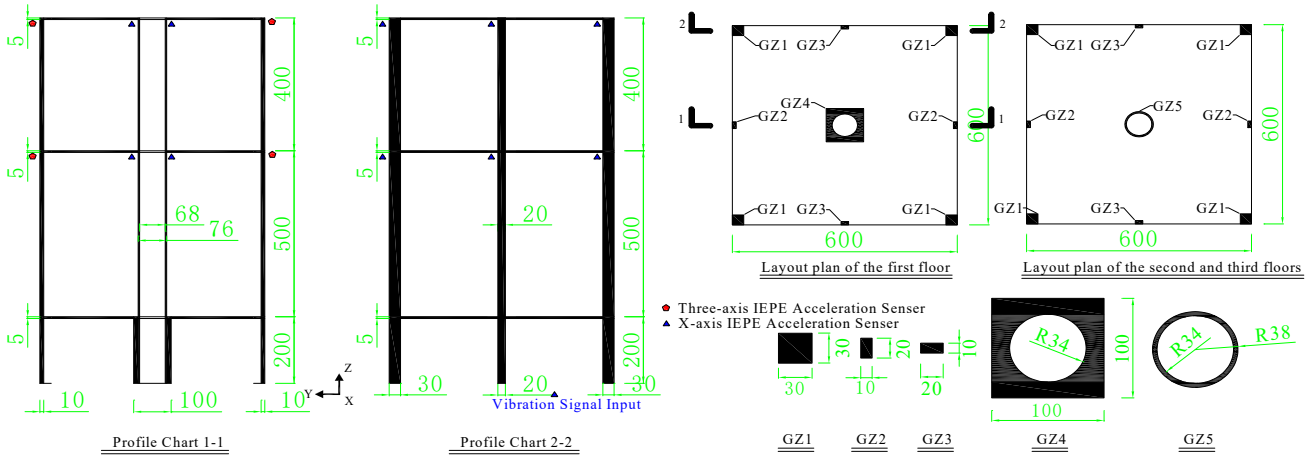

Fig. 9 The model's geometry and sensor placement

Table 1 Structural material parameters

Material	Modulus of elasticity E (GPa)	Density P (kg/m^3)	Poisson's ratio
Steel	200	7850	0.3

the middle of the middle and top levels simulate the thick concrete walls outside the generator. The properties of the main structures are listed in Table 1. The test data acquisition was performed using a National Instruments NI system with IEPE acceleration sensors to acquire the structural vibration signals. The structural model sensor arrangement and acquisition system is shown in Fig. 10.

Besides, the main factor causing the vibration of the PSPPs is the three-axis hydraulic vibration source, which leads to excessive vibration response in one direction in practical engineering. Its transmission path is gradually transferred to the superstructure through the worm shell, which excites the overall vibration of the structure. Therefore, this study only takes the upper structure as the research object, and only one direction horizontal excitation is considered in the test to study the overall structural vibration response under high frequency vibration of the structure. Through the test, we can better understand the high-frequency control method of the plant structure, which has some significance for the vibration control of the PSPPs plant structure.

To compare the effect of eddy current damping, controlled structures equipped with two damping devices are given as controls: undamped damper and eddy current damper. For the undamped TMD, the vibration energy of the structure can only be dissipated by vibration transfer to the TMD system. For EC-TMD, the vibration energy of the structure can also be dissipated by the eddy current damping of the dampers. Fig. 11 illustrates the eddy current damper test setup for vibration damping. The device is an eddy current damper consisting of a spring steel plate with a mass block and a magnet, a conductor copper plate with a magnetically conductive steel plate. It is attached to the structural column by a fixture to absorb the vibration energy of the structure and suppress the structural response. It should be noted that when the eddy current damping element is removed, the EC-TMD becomes an undamped TMD. Depending on the type of structure, the test model can be classified as an uncontrolled structure without

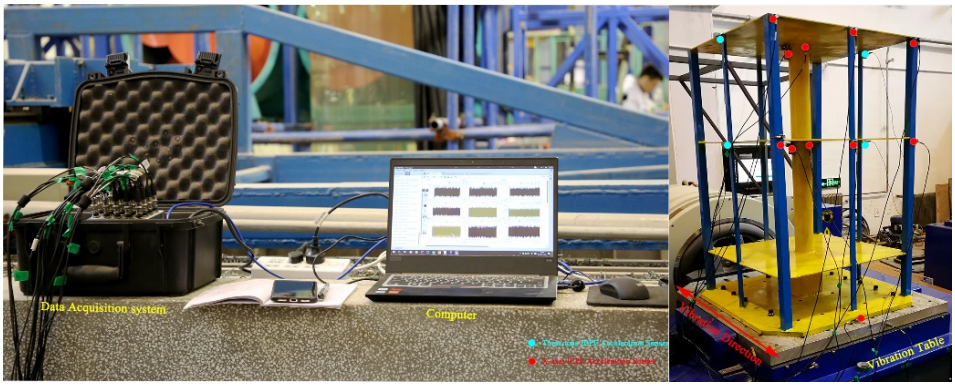

Fig. 10 Photos of the test model and acquisition equipment

Table 2 Vibration reduction test conditions

Excitation condition	Incoming signal	TMD position
STMD-T-COL	Harmonic Wave	Corner column of the top floor (Fig. a)
EC-STMD-T-COL	Harmonic Wave	Corner column of the top floor (Fig. b)
MTMD-T-COL	Harmonic Wave	Corner column of the top floor (Fig. c)
EC-MTMD-T-COL	Harmonic Wave	Corner column of the top floor (Fig. d)
MTMD-M-COL	Harmonic Wave	Corner column of the middle floor (Fig. e)
EC-MTMD-M-COL	Harmonic Wave	Corner column of the middle floor (Fig. f)
MTMD-T-MIN	Harmonic Wave	Middle column of the top floor (Fig. g)
EC-MTMD-T-MIN	Harmonic Wave	Middle column of the top floor (Fig. h)
MTMD-M-MIN	Harmonic Wave	Middle column of the middle floor (Fig. i)
EC-MTMD-M-MIN	Harmonic Wave	Middle column of the middle floor (Fig. j)
MTMD-T-STEEL	Harmonic Wave	Steel cylinder of the top floor (Fig. k)
EC-MTMD-T-STEEL	Harmonic Wave	Steel cylinder of the top floor (Fig. l)
MTMD-M-STEEL	Harmonic Wave	Steel cylinder of the middle floor (Fig. m)
EC-MTMD-M-STEEL	Harmonic Wave	Steel cylinder of the middle floor (Fig. n)

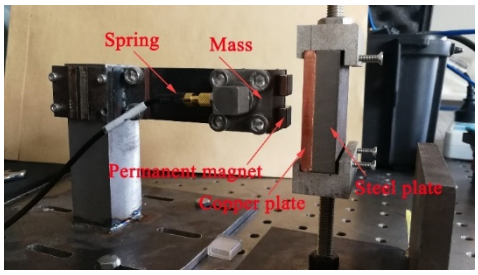

Fig. 11 Photo of eddy current TMD

a damper, a controlled structure with an undamped TMD, and a controlled structure with an EC-TMD.

The hydraulic source of the high-frequency vibration of the plant structure is simple harmonic, and the test uses high frequency simple harmonic to simulate the vibration response of different test models. EC-STMD consists of two parts, STMD and ECD. Therefore, the biggest difference between STMD and EC-STMD is that EC-STMD has a separate damping unit. Secondly, when arranging EC-STMD, in addition to the optimal arrangement of dampers, the ECD component also needs to be


(a) STMD-T-COL


(b) EC-STMD-T-COL


(c) MTMD-T-COL


(d) EC-MTMD-T-COL


(e) MTMD-M-COL


(f) EC-MTMD-M-COL


(g) MTMD-T-MIN


(h) EC-MTMD-T-MIN

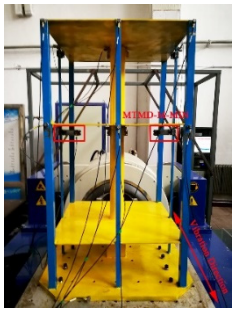
(i) MTMD-M-MIN


(j) EC-MTMD-M-MIN


(k) MTMD-T-STEEL


(l) EC-MTMD-T-STEEL


(m) MTMD-M-STEEL


(n) EC-MTMD-M-STEEL

Fig. 12 TMD layout diagram

considered. The different design conditions of the model tests are shown in Table 2. STMD-T-COL indicates a group of single TMDs arranged on the top corner column of the structure; EC-STMD-T-COL indicates a group of eddy current TMDs arranged on the top corner column of the structure; EC-MTMD-T-MIN indicates a group of eddy current MTMDs arranged on the top middle column of the structure; EC-MTMD-M-STEEL indicates that a group of eddy current MTMD is arranged on the steel cylinder in the middle layer of the structure; the nomenclature of the rest of the working conditions and so on. The design arrangement of vibration damping devices in the above test conditions is detailed in Fig. 12.

This section is studied to verify the feasibility and effectiveness of eddy current dampers. The peak value of the acceleration response of the structure under high-frequency excitation is given to evaluate its performance. The effectiveness of the damper is evaluated by the degree of attenuation of the maximum response of the structure. The damping rate is used to evaluate the vibration control performance of the system. The damping rate is defined as

$$VRR = \frac{P_u - P_t}{P_u} \tag{13}$$

Where P_u and P_t represent the peak acceleration responses of the uncontrolled and damped structures, respectively. Besides, the control effects of eddy current damping and undamped TMD, different control strategies and different arrangement positions on the peak acceleration are also analyzed and compared to comprehensively evaluate the performance of eddy current damping.

5. Results and analysis

5.1 Modal parameter identification

Modal parameter identification is the most important part of the test method process. The time-frequency

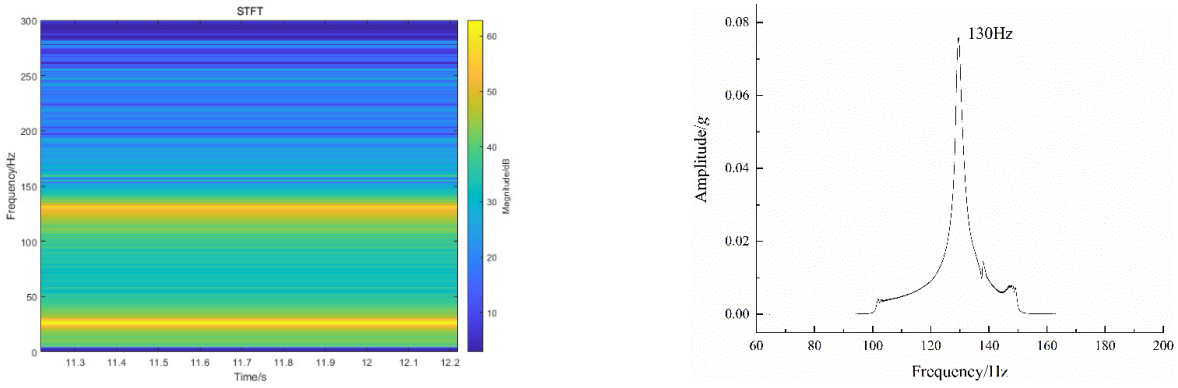

(a) (b)

Fig. 13 Modal parameter identification: (a) Time-frequency distribution of the original model; (b) The spectral curves of the higher-order modes

Table 3 Peak acceleration and vibration reduction rate of the model structure under harmonic excitation

Structure	Top (g)	Control effect (%)	Middle (g)	Control effect (%)
Uncontrolled	4.14		4.74	
STMD	0.97	76.52	1.54	67.55
EC-STMD	0.86	79.35	1.43	69.91
MTMD-T-COL	0.46	89.01	0.71	85.09
EC-MTMD-T-COL	0.43	89.52	0.70	85.28
MTMD-M-COL	0.27	93.53	0.31	93.46
EC-MTMD-M-COL	0.16	96.26	0.20	95.85
MTMD-T-MIN	0.46	88.84	0.81	83.03
EC-MTMD-T-MIN	0.46	88.96	0.72	84.84
MTMD-M-MIN	0.27	93.57	0.36	92.47
EC-MTMD-M-MIN	0.20	95.29	0.25	94.64
MTMD-T-STEEL	1.44	65.29	2.05	56.72
EC-MTMD-T-STEEL	0.86	79.18	1.22	74.26
MTMD-M-STEEL	0.71	82.95	0.91	80.81
EC-MTMD-M-STEEL	0.55	86.62	0.57	88.05

characteristics of the model structure are obtained by modal parameter identification. Fig. 13(a) shows the time-frequency curves of the structure under the X-directional sweep excitation. The figure shows that not only the first mode has a significant contribution to the structural response, but also the higher frequency modes at higher modes have a significant contribution to the structural response. In this paper, we focus on the vibration control scheme of the plant structure under high-frequency excitation, and therefore, we focus on the contribution of high-frequency excitation to the structural response. Fig. 13(b) shows the frequency domain curve of the fast Fourier transform amplitude of the structure. The higher-order mode of the structure corresponding to 130 Hz is a significant contribution to the structural response.

To study the vibration control effect of the damper-structure system under high-frequency excitation, the structure-TMD working effect under high-frequency excitation is analyzed by using the frequency corresponding to the second-order mode in the X direction of the structure as the excitation frequency. The control effects of different TMDs on structural high-frequency vibration are compared by comparing the peak values of structural response under high-frequency excitation of different operating conditions.

5.2 Effect of eddy current damping

Fig. 14 shows the time course curves of the top acceleration of the uncontrolled and controlled structures under high-frequency excitation. The peak acceleration response of undamped TMD and ECTMD is much smaller than that of the uncontrolled structure, indicating that TMD has a significant effect on reducing the peak acceleration of the structure, and both TMDs have good control effects. Due to the obvious role of eddy current damping in energy dissipation, the control of peak acceleration by undamped TMD is lower than that of EC-TMD.

Fig. 15 illustrates the peak acceleration responses of the top and middle layers of the uncontrolled and controlled structures. From the figure, the TMD arranged in the top layer of the structure can effectively control the high-frequency vibration of the structure. Whether it is an undamped TMD or an EC-TMD, when the TMD reaches the tuned operating frequency, the vibration energy of the structure is dissipated by vibration transfer to the TMD, and both TMDs can play a good tuned vibration reduction effect. The attenuation rate of the peak acceleration of the top layer of the undamped TMD structure is 76.52%, and the attenuation rate of the peak acceleration of the middle layer of the structure is 67.55%. As for EC-TMD, the energy dissipation can also be achieved by eddy current damping. Therefore, the vibration energy of the controlled structure can be effectively dissipated by EC-TMD in both tuned and detuned cases, which leads to the strong robustness of EC-TMD. the decay rate of the peak acceleration at the top layer of the EC-TMD structure is 79.35%, and the decay rate of the peak acceleration at the middle layer of the structure is 69.91%.

Fig. 16 illustrates the spectrum curve of the top layer of the uncontrolled and controlled structure. It can be seen from the figure that higher modes contribute significantly to the structural response, and when TMD is attached, the amplitude in the frequency domain is significantly mitigated, proving the effectiveness of TMD. It is also clear that EC-TMD controls the amplitude in the frequency domain better than undamped TMD due to eddy current damping. EC-TMD exhibits excellent damping over a wide frequency range, and the eddy current damping consumes energy from the vibration input, improving the robustness of the system.

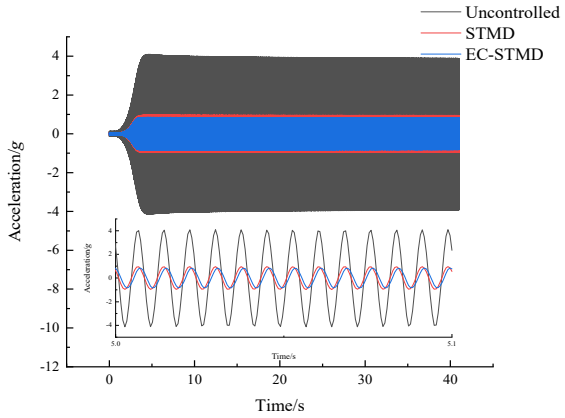

Fig. 14 Time-history curves of structural acceleration

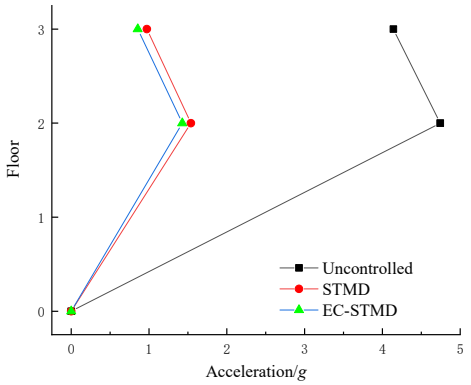

Fig. 15 Peak structural acceleration response

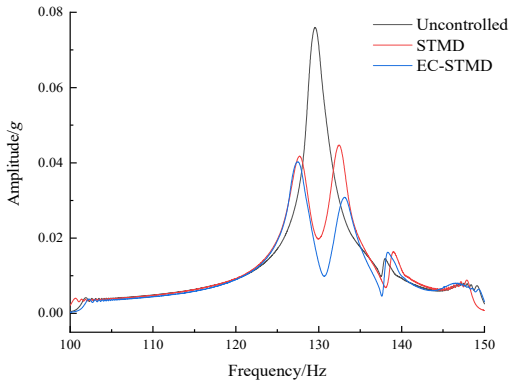

Fig. 16 Structural acceleration spectrum curve

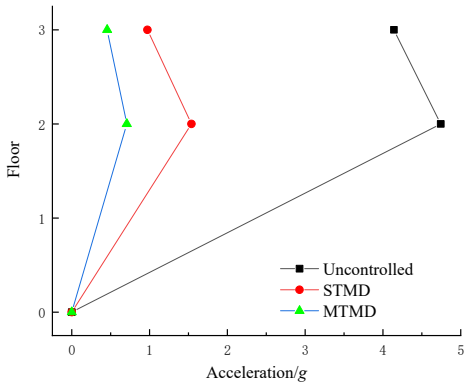

Fig. 17 Peak structural acceleration response with additional STMD and MTMD

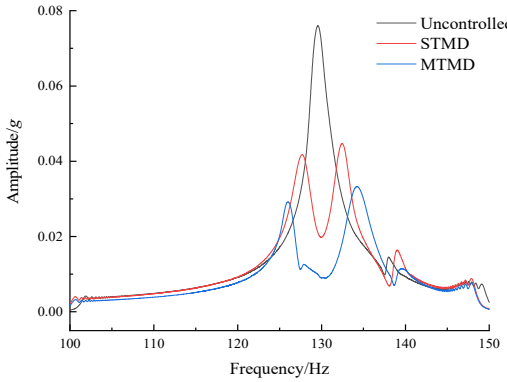

Fig. 18 Structural acceleration spectrum curves with additional STMD and MTMD

5.3 Effect of the control strategy

TMD provides excellent control of structural vibration. However, for complex structures, the control effect of a single TMD is limited. Therefore, this section compares the control effect of STMD and MTMD on the high-frequency vibration of the structure.

Fig. 17 shows the peak acceleration response of the top and middle layers of the structure without control and with additional STMD and MTMD. From the figure, the MTMD arranged at the top layer of the structure can control the high-frequency vibration of the structure more effectively than STMD, both for the vibration response at the top and middle layers of the structure. the decay rate of the peak acceleration at the top layer of the MTMD structure is 89.01%, and the decay rate of the peak acceleration at the middle layer of the structure is 85.09%. For MTMD, the control band widening increases the robustness of the system and improves the vibration effect of the structure.

Fig. 18 illustrates the spectral curves of the top layer of the uncontrolled and additional STMD and MTMD structures. From the figure, the peak amplitude of the structure with additional MTMD is significantly reduced, and the amplitude in the frequency domain is significantly

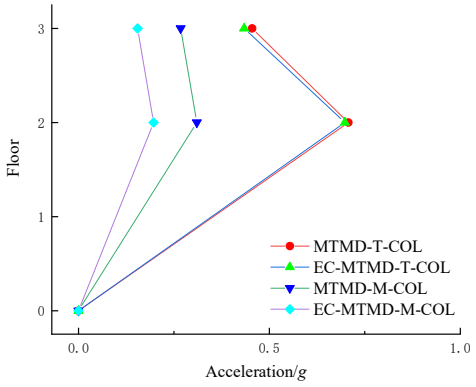

(a)

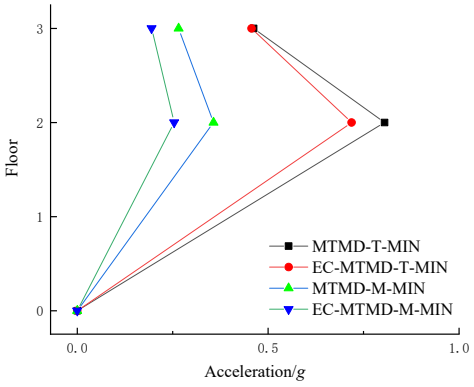

(b)

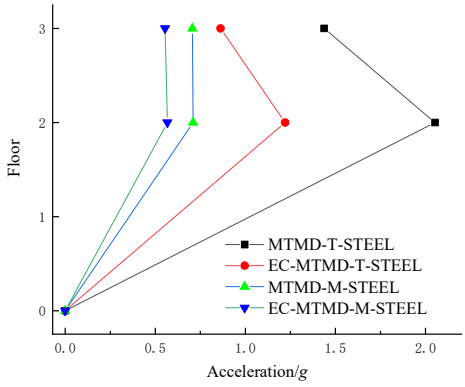

(c)

Fig. 19 Peak structural acceleration response with TMD at different floors: (a) Corner column; (b) Middle column; (c) Steel cylinder

better than the STMD control, which verifies the good vibration reduction performance of MTMD. It can also be seen that MTMD has better control of the bandwidth in the frequency domain than STMD, indicating that MTMD has better robustness and better anti-interference capability. Therefore, MTMD can better control the high-frequency vibration response of the structure.

5.4 Effect of layout floors

The ability of TMD to control the high-frequency vibration of structures has been proven. However, unlike controlling the vibration response of the structure at fundamental frequencies, the control effect of TMD arrangement at different floors is different for the control of high-frequency vibration of higher-order modes of the structure. In this section, undamped MTMD and EC-MTMD are selected to compare the control effects of MTMD arrangement at the top floor of the structure and the middle floor of the structure for different working conditions on the structural response, respectively.

Fig. 19(a) illustrates the structural peak acceleration response when the MTMD attached to the corner column is arranged at the top and middle floors of the structure, respectively. It can be seen from the figure that the peak acceleration of the floor with the MTMD arranged at the middle floor of the structure is significantly lower than that of the model with the MTMD arranged at the top floor of the structure, and the MTMD can effectively reduce the peak acceleration of the floor. Comparing the case of undamped MTMD arranged on the top and middle floors of the structure respectively, the peak acceleration decay rate of the top floor of the structure increases from 89.01% to 93.53%, and that of the middle floor of the structure increases from 85.09% to 93.46%. Comparing the case of EC-MTMD arranged at the top and middle floors of the structure respectively, the peak acceleration attenuation rate improved from 89.52% to 96.26% at the top floor of the structure and from 85.28% to 95.85% at the middle floor of the structure.

Fig. 19(b) illustrates the structural peak acceleration response when the MTMD attached to the middle column is arranged at the top and middle floors of the structure, respectively. It can be seen from the figure that the peak acceleration of the floor with the MTMD arranged at the middle level of the structure is significantly lower than that of the model with the MTMD arranged at the top level of the structure, and the MTMD can effectively reduce the peak acceleration of the floor. Comparing the case of undamped MTMD arranged on the top and middle floors of the structure respectively, the peak acceleration decay rate of the top floor of the structure increases from 88.84% to 93.57%, and the peak acceleration decay rate of the middle floor of the structure increases from 83.03% to 92.47%. Comparing the case of EC-MTMD arranged at the top and middle floors of the structure respectively, the peak acceleration attenuation rate increased from 88.96% to 95.29% at the top floor of the structure and from 84.84% to

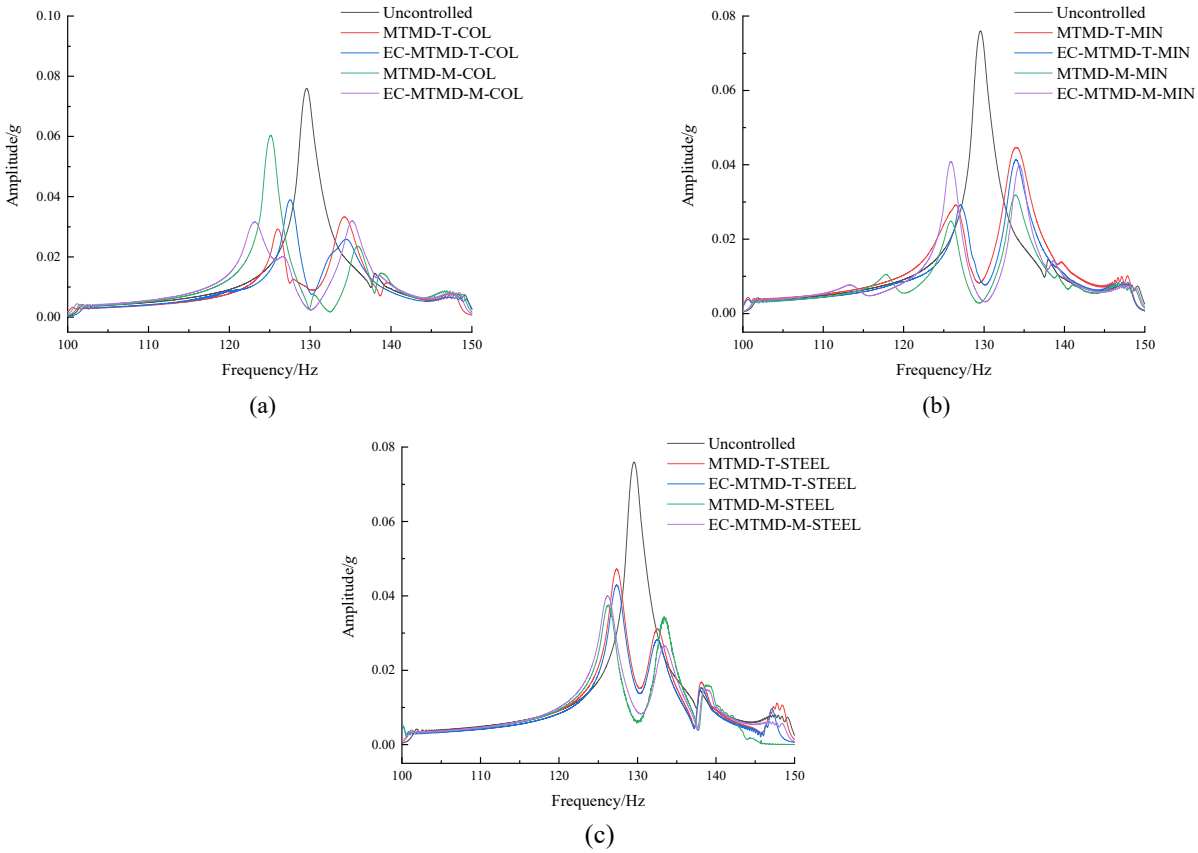

Fig. 20 Structural acceleration spectrum curves with TMD at different floors: (a) Corner column; (b) Middle column; (c) Steel cylinder

94.64% at the middle floor of the structure.

Fig. 19(c) illustrates the structural peak acceleration response when the MTMD attached to the steel cylinder is arranged at the top and middle floors of the structure, respectively. It can be seen from the figure that the peak acceleration of the floor with the MTMD arranged at the middle level of the structure is significantly lower than that of the model with the MTMD arranged at the top level of the structure, and the MTMD can effectively reduce the peak acceleration of the floor. Comparing the case of undamped MTMD arranged on the top and middle floors of the structure respectively, the peak acceleration decay rate of the top floor of the structure increases from 65.29% to 82.95%, and the peak acceleration decay rate of the middle floor of the structure increases from 56.72% to 80.81%. Comparing the case of EC-MTMD arranged at the top and middle floors of the structure respectively, the peak acceleration attenuation rate increased from 79.18% to 86.62% for the top floor of the structure and from 74.26% to 88.05% for the middle floor of the structure.

For the damping system, the damping effect is better in the middle layer of the structure compared with the corresponding dampers arranged in the top layer of the structure for the three different working conditions. Due to the eddy current damping, the damping advantage of the EC-MTMD comparison group is more obvious. The dampers are not placed at the top of the structure to achieve the best damping effect, especially for high-frequency vibration. The main reason for this is that high-frequency vibration often triggers higher-order modal resonance in the structure, where the maximum vibration pattern is not necessarily located at the top of the structure. Therefore, a TMD at the top may not achieve the desired control effect.

Fig. 20 show the spectral curves of the MTMD arranged in the top and middle layers of the structure, respectively. From the figures, the amplitude peak of the MTMD arranged in the middle layer of the structure is significantly lower and the amplitude in the frequency domain is significantly more controlled than that of the corresponding case arranged in the top layer. It is also clear that the EC-MTMD controls the bandwidth in the frequency domain better than the other cases. This is due to the strong robustness of EC-MTMD resulting from the effective dissipation of the vibration energy through eddy current damping. Overall, the EC-MTMD outperforms the undamped MTMD in both peak response reduction and the damping performance is optimized when the EC-MTMD is arranged at the position of maximum structural response.

5.5 Effect of position arrangement

In this section, undamped MTMD and EC-MTMD are selected to compare the control effects of different MTMD arrangement positions on the structural response, respectively. Fig. 21 illustrates the peak acceleration response of the structure with different MTMD arrangement

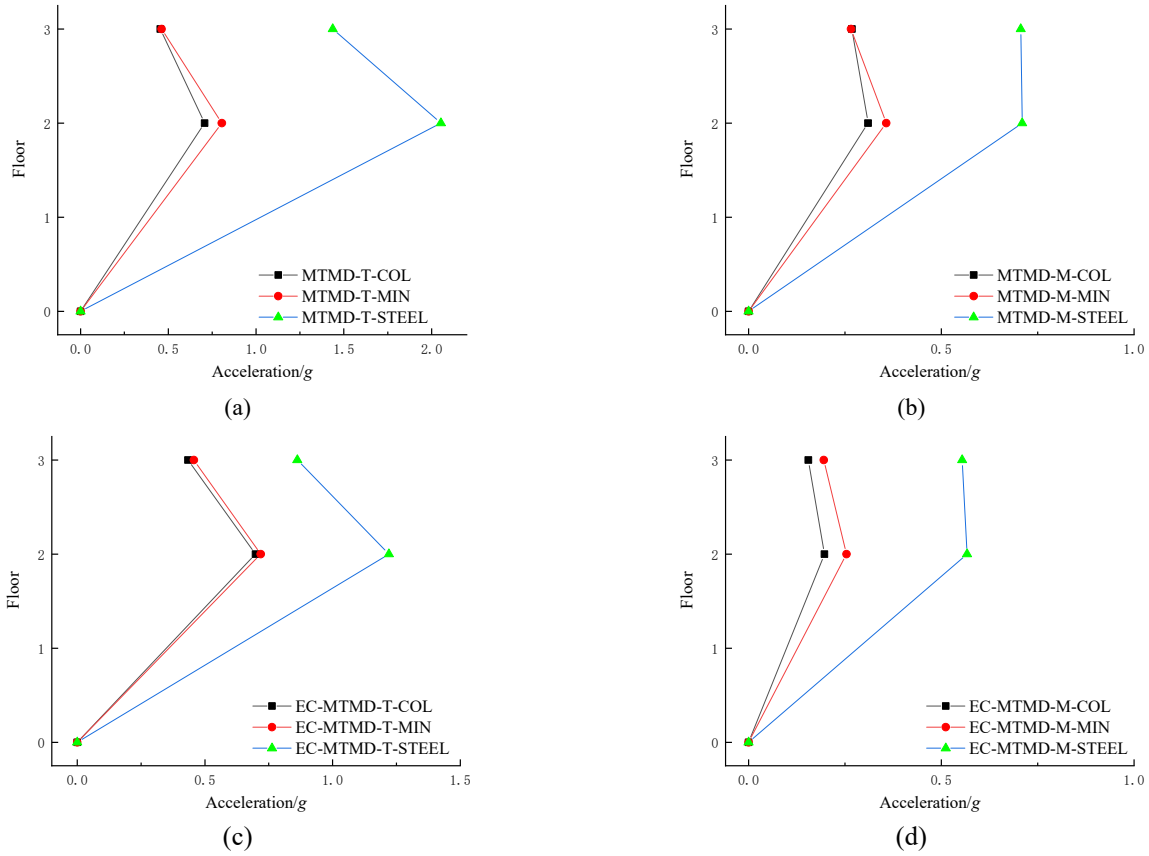

Fig. 21 Peak acceleration responses of structures with TMD at different locations: (a) MTMD placed at the top floor; (b) MTMD placed at the middle floor; (c) EC-MTMD placed at the top floor; (d) EC-MTMD placed at the middle floor

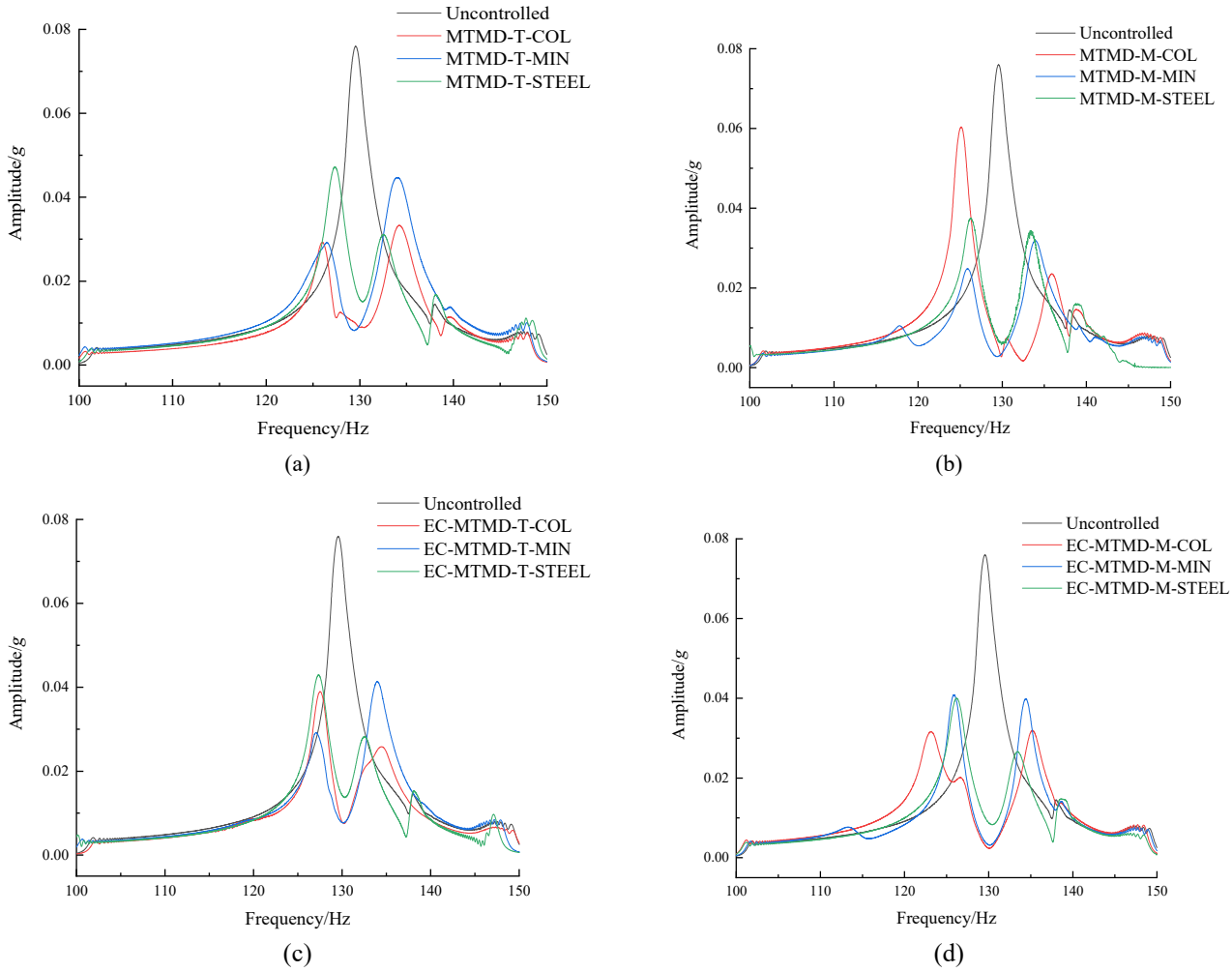

Fig. 22 Structural acceleration spectrum curves with TMD at different locations: (a) MTMD placed at the top floor; (b) MTMD placed at the middle floor; (c) EC-MTMD placed at the top floor; (d) EC-MTMD placed at the middle floor

positions. It can be seen from the figure that the control effect of the dampers arranged on the steel cylinder is lower than the other two arrangement schemes in both the cases of undamped MTMD and EC-MTMD. Although the MTMD arranged on the steel cylinder can reduce the peak acceleration of the plant structure, especially for the case of EC-MTMD, the control effect is still inferior to the other two schemes. The control effect of the arrangement scheme is arranged on the corner cone of the structure and the middle column of the structure is closed. In the case of undamped MTMD at the top of the structure, the peak acceleration decay rates are 89.01% and 88.84% at the top of the structure, and 85.09% and 83.03% at the middle of the structure, respectively; in the case of EC-MTMD at the top of the structure, the peak acceleration decay rates are 89.52% and 88.96% at the top of the structure, and 85.09% and 83.03% at the middle of the structure, respectively. The peak acceleration decay rates were 85.28% and 84.84% for the middle layer of the structure, respectively. In comparison, the EC-MTMD in the middle layer has the best control effect.

Fig. 22 shows the structural spectrum curves for different MTMD arrangement positions. It can be seen from the figure that all three schemes can reduce the amplitude peak of the structure, especially when eddy current is used. The amplitude of the MTMD scheme arranged on the steel cylinder is significantly higher than the other schemes when viewed at the high-frequency controlled frequency band. The difference between the amplitude of the remaining two schemes is not significant, which confirms the peak acceleration results. By using the eddy current control scheme, the EC-MTMD increases the frequency domain tuning bandwidth while controlling the amplitude in the frequency domain. Therefore, the scheme arranged on the corner and middle columns of the structure is more suitable than the scheme arranged on the steel cylinder.

For the damping system, the best damping effect is obtained for the three different arrangement schemes, arranged in the corner and center column of the structure, especially with eddy current damping. Due to the robustness of eddy current damping, the damping performance of EC-MTMD is better. For high-frequency vibration of the plant structure, the dampers are better arranged in the outer frame of the structure than inside the structure.

6. Conclusions

High-frequency vibration control of plant structure has been the key problem of vibration reduction in PSPPs. In this paper, a new eddy current TMD damping device is designed to address this problem, and a new EC-TMD-based high-frequency vibration damping control method is proposed to suppress the plant structure.

The influence law of different parameters of the new EC-TMD vibration damping device on the equivalent damping coefficient was analyzed by numerical simulation, and the designed EC-TMD model was evaluated systematically. And a series of physical model tests of the plant structure was carried out to verify the control effect of the eddy current dampers on the high-frequency vibration of the plant structure.

The effect of different parameters of the 3D electromagnetic field eddy current TMD on the equivalent damping coefficient varies. As the magnetic field gap decreases, the equivalent damping factor improves significantly. When the magnetic field gap is fixed, the equivalent damping coefficient increases with the increase of the residual flux density, slowly increases with the increase of the thickness of the conductor copper plate and the magnetic steel plate, and increases with the increase of the spacing between adjacent permanent magnets.

The physical model of the plant structure was tested on a shaking table, and the results showed that the new EC-TMD damping device is feasible and effective in suppressing the high-frequency vibration of the plant structure. From the structural top and middle floor acceleration response, the damping rate of the structural top floor acceleration reaches 79.35%. From different control strategies, the control effect of MTMD is significantly better than that of STMD. Besides, MTMD effectively increases the tuning band of the structural response and improves the robustness of the system. In addition, the suitable position will make the control effect more significant.

EC-TMD can be used for high frequency vibration control of related structures because of its excellent damping performance in suppressing high-frequency vibration of structures. However, the multi-axial vibration of complex hydraulic vibration sources needs further analysis. For the theory completeness, the multi-axial vibration of complex hydraulic vibration sources should be studied in the future.

References

Amjadian, M. and Agrawal, A.K. (2017), "A passive electromagnetic eddy current friction damper (PEMECFD): Theoretical and analytical modeling", *Struct. Control Health Monitor.*, **24**(10), e1978. https://doi.org/10.1002/stc.1978

Bakre, S.V. and Jangid, R.S. (2007), "Optimum parameters of tuned mass damper for damped main system", *Struct. Control Health Monitor.*, **14**, 448-470. https://doi.org/10.1002/stc.166

Bian, K. Liu, L., Xiao, M. and Liu, Z.Q. (2016), "Cause investigation and verification of lining cracking of bifurcation tunnel at Huizhou Pumped Storage Power Station", *Tunnel. Undergr. Space Technol.*, **54**, 123-134. https://doi.org/10.1016/j.tust.2015.10.030

Chang, C.C. (1999), "Mass dampers and their optimal designs for building vibration control", *Eng. Struct.*, **21**(5), 454-463. https://doi.org/10.1016/S0141-0296(97)00213-7

Ebrahimi, B., Khamesee, M.B. and Golnaraghi, F. (2009), "A novel eddy current damper: theory and experiment", *J. Phys. D: Appl. Phys.*, **42**(7), 075001. https://doi.org/10.1088/0022-3727/42/7/075001

Elias, S. and Matsagar, V. (2014), "Distributed multiple tuned mass dampers for wind vibration response control of high-rise building", *J. Eng.*, **2014**. https://doi.org/10.1155/2014/198719

Elias, S. and Matsagar, V. (2018), "Wind response control of tall buildings with a tuned mass damper", *J. Build. Eng.*, **15**, 51-60. https://doi.org/10.1016/j.jobe.2017.11.005

Frahm, H. (1909), "Device for damping vibrations of bodies", US Patent, US0989958.

Hartog, J.P.D. (1957), *Mechanical Vibrations*, John Wiley & Sons, Inc.

Kaldellis, J.K. and Zafirakis, D. (2007), "Present situation and future prospects of electricity generation in Aegean Archipelago islands", *Energy Policy*, **35**(9), 4623-4639. https://doi.org/10.1016/j.enpol.2007.04.004

Larose, G.L., Larsen, A. and Svensson, E. (1995), "Modelling of tuned mass dampers for wind-tunnel tests on a full-bridge aeroelastic model", *J. Wind Eng. Indust. Aerodyn.*, **54**, 427-437. https://doi.org/10.1016/0167-6105(94)00058-L

Li, Y. and Li, Y. (2005), "Analysis on the floor vibration of yantan hydroelectric generating station", *J. Shenyang Agricult. Univ.*, **36**(6), 713-717. [In Chinese]

Li, J.Y., Zhu, S. and Shen, J. (2019a), "Enhance the damping density of eddy current and electromagnetic dampers", *Smart Struct. Syst., Int. J.*, **24**(1), 15-26. https://doi.org/10.12989/sss.2019.24.1.015

Li, J.W., GU, Z.F., Zhu, H.F., Yu, J.X. and Ouyang, J.H. (2019b), *Study on intense vibration of local structures of Zhanghewan pumped-storage powerhouse*, IOP Publishing. https://doi.org/10.1088/1755-1315/240/8/082008

Luo, X., Guo, P., Liu, S., Liao, W. and Zheng, X. (2006), "Research on vibration reducing measures of large size Francis turbine unit", *WSEAS Transact. Fluid Mech.*, **1**(5), 423-430.

Ma, Z.Y. and Wu, Q.Q. (2016), "The dynamic analysis of hydropower house and unit system in coupled hydraulic-mechanical-electric factors", *Proceedings of IOP Conference Series: Earth and Environmental Science*, **49**(5), 052011. https://doi.org/10.1088/1755-1315/49/5/052011

Ma, Z.Y., Shen, C.N., and Wang, Y.B. (2001), "Studies on the Anti-vibration and Reinforcement of Powerhouse in Hongshi Hydropower Station", *J. Hydroelect. Eng.*, **1**, 28-36. [In Chinese]

Marian, L. and Giaralis, A. (2017), "The tuned mass-damper-inerter for harmonic vibrations suppression, attached mass reduction, and energy harvesting", *Smart Struct. Syst., Int. J.*, **19**(6), 665-678. https://doi.org/10.12989/sss.2017.19.6.665

Matsuzaki, Y., Ikeda, T., Nae, A. and Sasaki, T. (2000), "Electromagnetic forces for a new vibration control system: Experimental verification", *Smart Mater. Struct.*, **9**(2), 127-131. https://doi.org/10.1088/0964-1726/9/2/301

Mohanta, R.K., Chelliah, T.R., Allamsetty, S., Akula, A. and Ghosh, R. (2017), "Sources of vibration and their treatment in hydro power stations-A review", *Eng. Sci. Technol.*, **20**(2), 637-648. https://doi.org/10.1016/j.jestch.2016.11.004

Niu, H.W., Chen, Z.Q., Hua, X.G. and Zhang, W.Z. (2018), "Mitigation of wind-induced vibrations of bridge hangers using tuned mass dampers with eddy current damping", *Smart Struct. Syst., Int. J.*, **22**(6), 727-741. https://doi.org/10.12989/sss.2018.22.6.727

Pan, Q., He, T., Xiao, D.H. and Liu, X.D. (2016), "Design and

Damping Analysis of a New Eddy Current Damper for Aerospace Applications", *Latin Am. J. Solids Struct.*, **13**(11), 1997-2011. https://doi.org/10.1590/1679-78252272

Perez-Sanchez, M., Sanchez-Romero, F.J., Ramos, H.M. and Lopez-Jimenez, P.A. (2017), "Energy recovery in existing water networks: Towards greater sustainability", *Water-Sui*, **9**(2), 97. https://doi.org/10.3390/w9020097

Qian, Z.D., Yang, J.D. and Huai, W.X. (2007), "Numerical simulation and analysis of pressure pulsation in Francis hydraulic turbine with air admission", *J. Hydrodyn.*, **19**(4), 467-472. https://doi.org/10.1016/S1001-6058(07)60141-3

Ramezani, M., Bathaei, A. and Zahrai, S.M. (2017), "Designing fuzzy systems for optimal parameters of TMDs to reduce seismic response of tall buildings", *Smart Struct. Syst., Int. J.*, **20**(1), 61-74. https://doi.org/10.12989/sss.2017.20.1.061

Rehman, S., Al-Hadhrami, L.M. and Alam, M.M. (2015), "Pumped hydro energy storage system: A technological review", *Renew. Sustain. Energy Rev.*, **44**, 586-598. https://doi.org/10.1016/j.rser.2014.12.040

Seleznev, V.S., Liseikin, A.V., Bryksin, A.A. and Gromyko, P.V. (2014), "What Caused the Accident at the Sayano–Shushenskaya Hydroelectric Power Plant (SSHPP): A Seismologist's Point of View", *Seismol. Res. Lett.*, **85**(4), 817-824. https://doi.org/10.1785/0220130163

Sodano, H.A. and Bae, J.S. (2004), "Eddy current damping in structures", *Shock Vib. Digest*, **36**(6), 469-478. https://doi.org/10.1177/0583102404048517

Sodano, H.A., Bae, J.-S., Inman, D.J. and Keith Belvin, W. (2005), "Concept and model of eddy current damper for vibration suppression of a beam", *J. Sound Vib.*, **288**(4), 1177-1196. https://doi.org/10.1016/j.jsv.2005.01.016

Sun, X.S., Wang, X.G., Liu, L.P. and Fu, R.Z. (2019), "Development and present situation of hydropower in China", *Water Policy*, **21**(3), 565-581. https://doi.org/10.2166/wp.2019.206

Thomson, W.T. (1972), *Theory of vibration with applications*. Prentice-Hall.

Tributsch, A. and Adam, C. (2012), "Evaluation and analytical approximation of Tuned Mass Damper performance in an earthquake environment", *Smart Struct. Syst., Int. J.*, **10**(2), 155-179. https://doi.org/10.12989/sss.2012.10.2.155

Tsioliaridou, E., Bakos, G.C. and Stadler, M. (2006), "A new energy planning methodology for the penetration of renewable energy technologies in electricity sector—application for the island of Crete", *Energy Policy*, **34**(18), 3757-3764. https://doi.org/10.1016/j.enpol.2005.08.021

Wang, L.K., Shi, W.X., Zhou, Y. and Zhang, Q.W. (2020), "Semi-active eddy current pendulum tuned mass damper with variable frequency and damping", *Smart Struct. Syst., Int. J.*, **25**(1), 65-80. https://doi.org/10.12989/sss.2020.25.1.065

Warburton, G.B. (1982), "Optimum absorber parameters for various combinations of response and excitation parameters", *Earthq. Eng. Struct. Dyn.*, **10**(3), 381-401. https://doi.org/10.1002/eqe.4290100304

Warnitchai, P. and Hoang, N. (2006), "Optimal placement and tuning of multiple tuned mass dampers for suppressing multi-mode structural response", *Smart Struct. Syst., Int. J.*, **2**(1), 1-24. https://doi.org/10.12989/sss.2006.2.1.001

Wen, Q., Hua, X.G., Chen, Z.Q., Yang, Y. and Niu, H.W. (2016), "Control of human-induced vibrations of a curved cable-stayed bridge: design, implementation, and field validation", *J. Bridge Eng.*, **21**(7). https://doi.org/10.1061/(ASCE)BE.1943-5592.0000887

Wiesner, K.B. (1979), *Tuned Mass Dampers to Reduce Building Wind Motion*, ASCE, New York.

Zhang, Y.N., Zheng, X.H., Li,J.W. and Du, X.Z. (2018), "Experimental study on the vibrational performance and its physical origins of a prototype reversible pump turbine in the pumped hydro energy storage power station", *Renew. Energy*, **130**, 667-676. https://doi.org/10.1016/j.renene.2018.06.057

BS